Mixing Dynamics in Interacting Vortices

Saptarshi Basu, Swetaprovo Chaudhuri, Baki M. Cetegen and Abhishek Saha

Abstract Mixing dynamics arising from the interaction of two convecting line vortices of different strengths and time delays have been investigated in this chapter. Experimentally obtained planar laser induced fluorescence images of acetone vortices mixing in air are thoroughly substantiated with computational modeling and analysis. Same and opposite direction of rotation, generating vortex pairs and couples were found to augment and dissipate species mixing respectively as indicated by global scalar statistics like mean and variance. Local mixing characteristics are analyzed using joint probability density function of vorticity and species concentration. This quantitatively showed how mixing is dissipated or augmented for individual vortices and at different vorticity magnitudes, even by the decaying and apparently indiscernible presence of a favorable or unfavorable direction of rotation of the preceding vortex.

1 Introduction

Flow induced mixing of different fluids (gas or liquid) is a fundamental process in many natural and engineered applications [1–10]. As an example, turbulent mixing

S. Basu (✉)
Department of Mechanical Engineering, Indian Institute
of Science Bangalore, Bengaluru, India
e-mail: sbasu@iisc.ac.in

S. Chaudhuri
Department of Aerospace Engineering, Indian Institute
of Science Bangalore, Bengaluru, India

B. M. Cetegen
Department of Mechanical Engineering, University
of Connecticut Storrs, Connecticut, USA

A. Saha
Department of Mechanical and Aerospace Engineering,
Princeton University, Princeton, NJ, USA

is ubiquitous in nature and is employed in many thermal systems such as fuel pre-mixers, gas turbine combustion chambers, etc. Interacting vortices/eddies constitute units of turbulence and hence are abundantly seen in physical sciences like in atmospheric studies, thermal plumes [10], volcanoes, engineering applications like bluff body separated flows, microfluidics and biological processes like cardiac flows or propulsion mechanism of sea mammals. These vortices can be of different strengths and sizes. Organized, coherent vortices and their interactions assist in scalar transport and mixing augmentation in both reacting and non-reacting flows encountered in different applications [10].

One methodology commonly adopted in order to achieve an in-depth understanding of the complicated mixing dynamics in turbulent flows, has been to study the mixing characteristics in a flow field perturbed by vortical structures such as isolated vortices and interacting vortices such as vortex pairs, vortex couples, etc. Controlled interaction of vortices of a given strength and timing serves an important problem in understanding the fundamental steps to understand mixing processes in turbulent scalar transport.

Passive scalar mixing by vortices in non-reacting convective diffusive flows have been a subject of continued interest in the fluid dynamics community. Excellent reviews on the analysis of vortical flows can be found in the works of Renard et al. [10]. The complexity of mixing phenomenon introduced in the domain of a vortical flow makes this an active research area as of date as evidenced by many recent works on this subject. Villermaux and Duplat [11] showed mixing by aggregation in an experimental study of a stirred scalar reactor. Meunier and Villemaux [12] described the mixing phenomenon in a vortex by considering advective-diffusive behavior of a scalar blob in the deformation field of an axisymmetric vortex. Bajer et al. [13] analytically studied the mixing in a vortex with focus on the enhancement of scalar destruction at the vortex core. In microfluidic devices operating at a regime of very low Reynolds number, vortex interaction is a widely used method for passive mixing. Recently, Long et al. [14] discussed the usage of vortical flows in a 3D micro mixer. Sritharan et al. [15] also used vortex induced flows to enhance mixing in microchannels. They used acoustic pulses to generate streaming within the flow, which resulted in interacting vortices enhancing mixing.

Motivated by these computational, analytical and experimental studies, we previously reported a computational study [16] of vortical mixing in a gaseous flow field in the same experimental configuration of Cetegen [17]. However, the previous experimental and computation efforts involved scalar mixing analysis in a single isolated vortex. A more useful and fundamental problem is the fluid mechanics and mixing characteristics of interaction of two interacting vortices created in a laminar diffusion layer in the same experimental configuration of Cetegen [17]. This chapter concerns qualitative experimental results substantiated with the computational modeling and quantitative analysis. The modeling effort used the same experimental configuration for the ease of qualitative comparison. In the following sections, we first describe the experimental methods followed by a brief description of the computational model.

2   Problem Description: Experimental and Computational

An experimental and computational study of scalar mixing in the field of two successively generated counter rotating laminar vortices at the interface of two gas streams (one seeded with acetone and another unseeded) flowing parallel to each other in a rectangular flow channel is presented (Fig. 1). The isolated vortex evolutions and mixing in the field of a single vortex has been studied in detail by Cetegen [17]. In this study, a line vortex was initiated by rapidly increasing one of the stream velocities in relation to the other in otherwise equal velocity, co-flowing streams separated upstream by a splitter plate (Fig. 1a). Using planar laser induced fluorescence of acetone, the mixing field was characterized in terms of probability density distributions of the passive scalar and its moments. In the present study, a second vortex rotating in the opposite direction is created in a similar fashion in the other or the same gas stream with variable time lag with respect to the first vortex (Fig. 1a). Interacting vortices introduced in opposite streams are referred to as vortex couple (studied both experimentally and computationally) while the vortex generated in the same gas stream is called vortex pair (only studied computationally). The dynamics of the interacting vortices depends on several key variables, namely a.) the relative strengths (A1/A2 in Fig. 1a), the time delay between the introduction of the two vortices and c.) the side from which the second vortex is introduced (vortex pair or couple).

Planar laser induced fluorescence of acetone is utilized to visualize the scalar concentration distribution in this flow field. Similar flow field and scalar distribution was analyzed using a computational model to quantify the mixing dynamics in dual vortex configuration. A parametric study was conducted to determine the effects of time lag and convection time on scalar mixing characteristics in the interaction zone of the two vortices. Figure 1a top (bottom) row shows the configuration in which the second vortex is introduced on the opposite (same) side as the first vortex with a controlled phase lag. Commercial code fluent 6.3.16 was used for all the computational simulations. Using experiments and computations, we have attempted to visualize and analyze the mixing dynamics in a flow field of interacting vortices, respectively.

2.1   Experimental Setup

The experimental setup and methodology has been described by Cetegen [17] in details and is restated here for completeness. The same experimental setup [17] was modified to account for the generation of two vortices. The experimental setup [17] comprises of a two dimensional convergent nozzle divided into two equal zones by a splitter plate as schematically shown in Fig. 1b. The dimension of each nozzle segment is 2.0×6.0 cm at the exit plane. The optical test section which extends beyond the nozzle exit is enclosed by four quartz windows (10 cm long). Flow conditioning
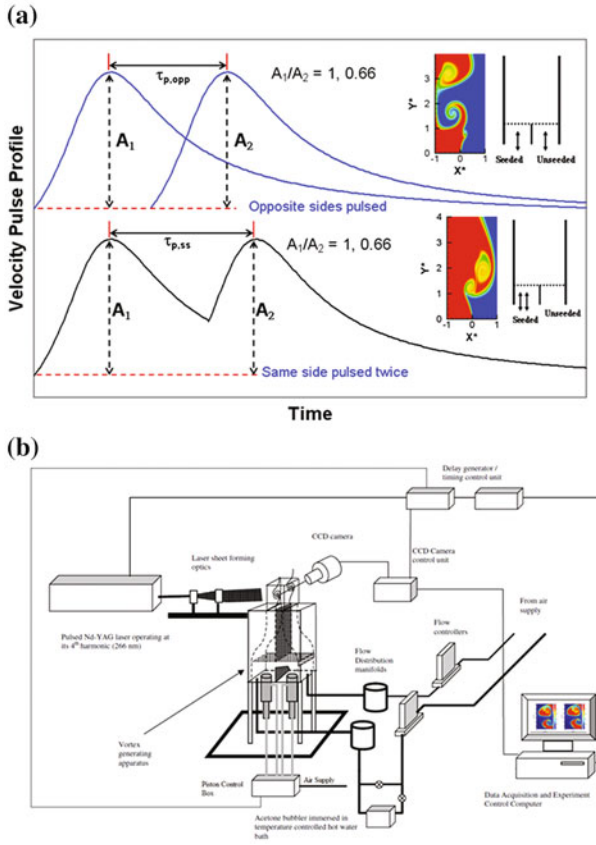
Fig. 1 **a** Pulse profiles (same side [vortex pair] and opposite sides [vortex couple]) for generating the interacting vortices, **b** Experimental setup for laser induced fluorescence of acetone (Adapted from 17)

is accomplished in the nozzle section using multiple layers of honeycombs and wire meshes. At the bottom of both of the chambers were 5 cm diameter cylindrical volumes into which two Teflon pistons (one for each chamber) were fitted. The Teflon pistons were actuated by electro pneumatic solenoids with a maximum stroke length of 26 mm. Different magnitudes of air pressure actuating the solenoid valves were utilized to initiate vortices with different magnitudes of circulation. Both the nozzle sections (for seeded and unseeded flow) were fed separately by metered compressed dry bottled air (Airgas industrial grade) using electronic mass flow controllers (Porter Instruments, Model 202). One of the air streams was partially bypassed and bubbled through an acetone filled container that was maintained at a constant temperature of 60 °C by immersing into a temperature controlled water bath (Fischer Scientific, Isotemp 105). This resulted in effective seeding of one of the air stream. Dynamic adjustment and control of the water bath temperature and flow bypass was carried

out to ensure LIF signal with good signal to noise ratio. The vortex generation was initiated from both the acetone-seeded air stream and the unseeded air stream at different levels of phase lags.

2.1.1 Planar Laser-Induced Fluorescence of Acetone

Laser induced fluorescence from acetone vapor was used as the preferred experimental technique in this study [17]. Normally seeding the flow with particles (like smoke) and using Mie scattering for concentration measurement is not a suitable technique for the current study. Smoke does not exhibit molecular diffusion and hence is not an inappropriate marker of mixing dynamics. Acetone fluorescence was selected because it acts as a molecular tag with diffusivity similar to the self-diffusion coefficient of air. Laser induced acetone fluorescence has been widely used for concentration and temperature measurements in both reacting and non-reacting gas flows. In this implementation as described by Cetegen [17], the fourth harmonic beam ($\lambda =$ 266 nm) of a pulsed Nd-YAG laser (Continuum YG-681-10) was expanded to form a 100 μm thick, 30 mm high laser light sheet. The laser sheet illuminated the mid-span of the flow in the optically accessible section of the experimental setup (Fig. 1b). The laser pulse duration was about 10 ns while the pulse energy was about 17–20 mJ. The fluorescence was collected using f = 2.8 optics onto a 1024×1024 pixel CCD camera (PI-MAX) coupled to an external intensifier (GEN2, P43). The vortex generation and image acquisition tasks were synchronized using two electronic delay generators (Stanford Instruments Model DG 535). Piston motion and velocity were measured by a monochromatic high speed camera, Motion Scope (Redlake Imaging, Model 8000), to determine the linear motion of the marked piston shafts for different phase lags between the two pistons profiles to undertake a parametric study of the vortical interaction as a function of time lag between their generation. Sample PLIF images are shown in Fig. 2 with their computational counterparts (described later).

The timing of the vortex imaging has been shown in Fig. 3. The laser fire signal at 10 Hz was used as the master signal to coordinate the experiment's timing. The camera and the intensifier were phase locked to the laser pulse using one delay generator (DG1) capturing every fourth pulse due the readout time delay. Vortex generation in both the chambers were initiated by externally triggering the electro pneumatic piston solenoid controller slaved to the laser fire signal by using a second delay generator (DG2) pulsed by the first delay generator (DG1) controlling the camera. The time delay between the initiations of the two vortex pulses, i.e. delay between the respective motion starting times between two pistons, were also adjusted using the second delay generator (DG2) and this delay will be called phase lag on delay generator $\Delta\tau_{p1-p2}$ henceforth. Another time delay was introduced for the camera and intensifier gate to coincide with one of the laser pulses illuminating the vortex in the test section. The time delays between DG1 and DG2 were slowly varied to capture vortices at different convection distances in the test section. Detailed timing diagram for a particular case $\Delta\tau_{p1-p2} = 0.015$ s is shown in Fig. 3. The study is primarily restricted to the visualization of the acetone PLIF contours and more
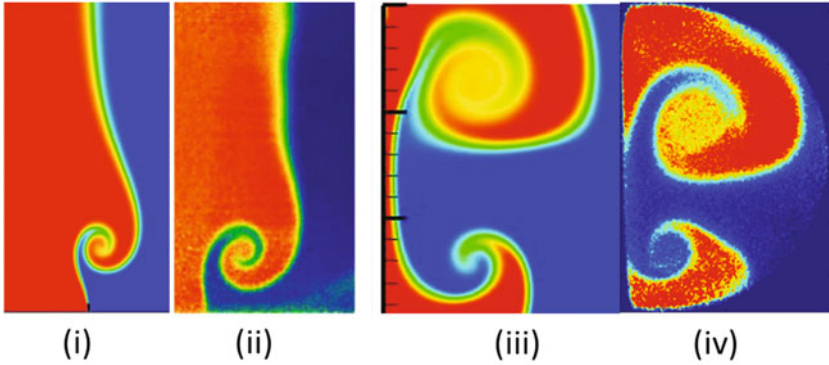
Fig. 2 i Species concentration (mass fraction) contour for single vortex (computational) [16], **ii** Species concentration (mass fraction) contour for single vortex (experimental) [17], **iii** Species concentration (mass fraction) contour for interacting vortices (computational), **iv** Species concentration (mass fraction) contour for interacting vortices (experimental)
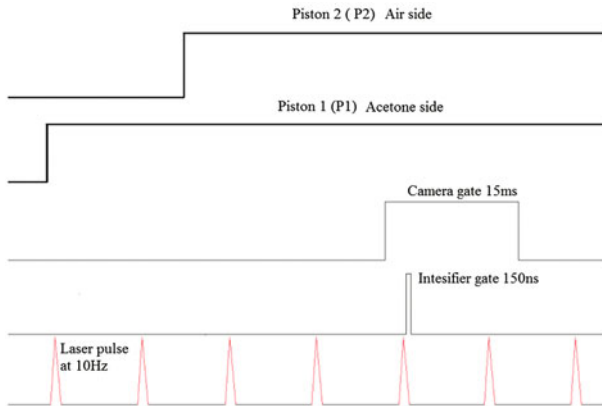

Fig. 3 Timing diagram for a sample vortex couple, $\tau_{P1-P2} = 0.015$ s

detailed mixing analysis based on behavior of concentration pdfs or joint pdfs is left for a future study. Figure 4 shows the P1 and P2 velocity at different $\Delta\tau_{p1-p2}$. It can be seen that the piston pulse profiles show reasonably good similarity with the theoretical pulse profiles (used in the computational study) shown in Fig. 1a. The peak values, growth and decay rates of the experimental pulse profile (Fig. 4) are also similar to that of the theoretical counterpart (Fig. 1a).
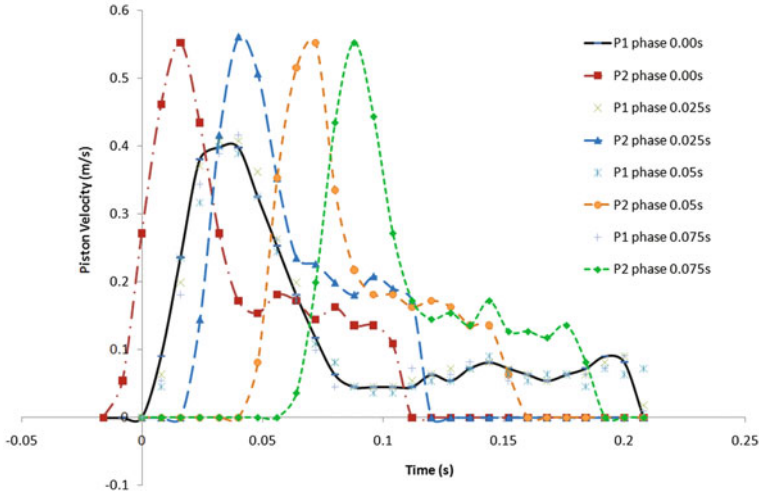
Fig. 4 Piston velocity time series

2.2 Computational Model

The computational model presented here and in our earlier work [16] simulates the laminar diffusion layer/wake formed by two gaseous flow streams (air in this case) having similar velocities being brought together at the trailing edge of a splitter plate as described in the previous section. The computational pulse profiles (Fig. 1a) mimics the volumetric displacement of a piston in the flow chamber used to create the line vortex in the experiments.

The extent of interaction of the vortices is a function of the time lag of the vortex generating pulses and their strengths. The mixing induced by the vortices is also dependent on the vortex configurations of vortex couple (opposite sign) or vortex pair (same sign) as indicated in Fig. 1a.

The governing equations for unsteady two-dimensional flow field in normalized form have been reported by Basu et al. [16] and are briefly restated here for clarity.

$$\text{Continuity:} \quad \frac{\partial \tilde{\rho}}{\partial t*} + \nabla \cdot [\tilde{\rho}\tilde{V}] = 0 \tag{1}$$

$$\text{Momentum:} \quad \tilde{\rho}\frac{\partial \tilde{V}}{\partial t*} + (\tilde{\rho}\tilde{V} \cdot \nabla)\tilde{V} = -Eu\nabla\tilde{P} + \frac{1}{\text{Re}}\nabla[\tilde{\mu}\nabla\tilde{V}] \tag{2}$$

$$\text{Species:} \quad \frac{\partial \tilde{Y}}{\partial t*} + \tilde{V} \cdot \nabla\tilde{Y} = \frac{1}{\text{Re}Sc}\nabla \cdot (\tilde{D}\nabla\tilde{Y}) \tag{3}$$

$$\text{Energy}: \quad \frac{\partial \tilde{T}}{\partial t*} + \tilde{V} \cdot \nabla \tilde{T} = \frac{1}{\text{Re}\,\text{Pr}} \nabla \cdot (\tilde{k}\nabla \tilde{T}) \tag{4}$$

where $\tilde{V} = [u/U_c, v/U_c]$ is the normalized velocity vector with u and v being the velocity components in the stream wise and cross stream directions. The convective velocity of the gas streams on either side of the splitter plate was denoted as U_c, which is the nominal velocity of the flow before the application of the pulse. $t* = tU_c/w$, $\tilde{\rho} = \rho/\rho_a(T_o)$, $\tilde{P} = P/P_o$, $\tilde{Y} = Y/Y_{s,i}$, and $\tilde{T} = T/T_o$ are the normalized time, density, pressure, mass fraction of the seed, and temperature, respectively, with $P_0 = 1$ atm and $T_0 = 300$ K [16]. Subscripts "a" and "s" refer to the unseeded air stream and acetone seeded air stream as in the experiments [16, 17]. "i" denotes the inlet values [16]. Transport coefficients $\tilde{\mu} = \mu/\mu_a(T_o)$, $\tilde{D} = D_{s,a}/[D_{s,a}(T_o)]$ and $\tilde{k} = k/k_a(T_o)$ are all normalized with their values at the reference temperature $T_0 = 300$ K. The non-dimensional quantities appearing in the governing equations are Euler number, $Eu = P_o/(\rho_a U_c^2)$, Reynolds number, $\text{Re} = (\rho_a U_c w)/\mu_a$, Schmidt number, $Sc = v_a/D_{s,a}$, and Prandtl number, $\text{Pr} = v_a/\alpha_a$ all evaluated at T_0. Convection velocity, U_c and channel width, w were utilized in the normalization [16]. Velocity, U_c at the two inlets (seeded or unseeded in Fig. 1a) was constant across the channel width before the initiation of the vortex generating velocity pulses. The transient velocity pulse profiles shown in Fig. 1a is provided as input boundary conditions to the above model. Further details of the numerical schemes used, boundary conditions, mesh size selection and convergence could be found in the work on single vortex mixing by Basu et al. [16]. The one gas stream is assumed to be seeded with acetone at a mass fraction of 0.25 at the exit plane.

The mixing enhancement as seen visually in Fig. 2 (evidenced in both experiments and computations) has been analyzed using two methods as will be described later. τ_p is defined as physical time delay normalized by convective time scale (w/U_c).

It is to be noted that the experimental and computational data show good agreement for the single vortex as shown in Fig. 2, parts i–ii. For the interacting vortices, the experimental and computational data show reasonably good agreement as well (Fig. 2, parts iii–iv).

3   Experimental Observations

In this section, a parametric experimental study of the double vortex interaction based on varying τ_{P1-P2} is presented. The time difference between the occurrence of peak velocities of P1 and P2 will be referred to as $t_{p,exp}$ henceforth. It is to be recognized that $t_{p,exp}$ (time difference between peak piston velocities) is not equal to the τ_{P1-P2} (time difference between input TTL signals, hence the different notations) in general due to slightly different inertia of the piston actuation systems. For most cases we found $\tau_{P1-P2} = t_{p,exp} + 0.025$ s.

Figure 5 shows the mixing layer formed between the acetone and air stream in the absence of vortex generating pulses. The rounding off at the top and bottom is
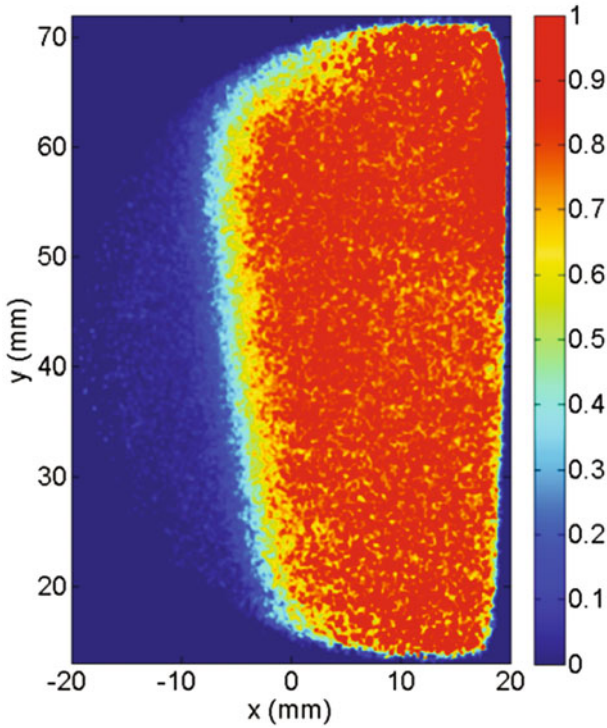
Fig. 5 Mixing layer between acetone and air streams

attributed to the clipping due to the circular intensifier field of view. Figure 6 shows the evolution of a single vortex rotating clockwise created by pulsing the acetone side. First proceeding along the top row, left to right: any image is obtained 2 ms after its immediate left neighbor showing the evolution and convection of the vortex along the other stream. The pulse strength is intentionally made stronger than that for a well formed vortex such that during its interaction with the counter-rotating vortex as studied subsequently, its vorticity is not dissipated to negligible values. Figure 7 shows the counterclockwise rotating vortex pulsed from the air side. These are very similar to those reported by Cetegen [17]. These two figures (Figs. 6 and 7) show the isolated vortex evolution, all the parameters of these are individually identical to their interacting counterparts described hence-forth. Figure 8 shows the evolution of two interacting vortices for $\tau_{P1-P2} = 0.075$ s. First the acetone side is pulsed and 0.075 s afterwards the air side is pulsed creating two counter-rotating vortices. It is observed that the time delay of $\tau_{P1-P2} = 0.075$ s, and $t_{p,exp} = 0.05$ s is too long to create a strong interaction between the two vortices, given the observation that coherent vortex structures of the individual vortices are preserved. However, it could be observed that the circulation strength which could be considered proportional to the growth rate of their diameters is reduced in comparison to their isolated counterparts as shown
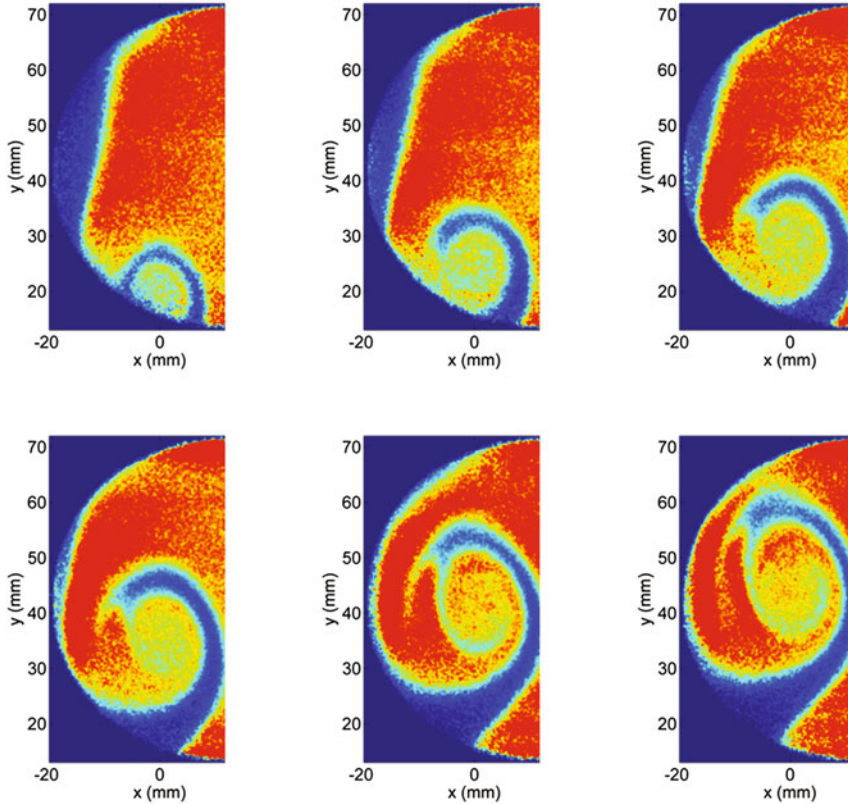
Fig. 6 PLIF profiles for acetone side pulsed vortex

in Figs. 4 and 5. Figure 9 shows remarkable repeatability of the interaction images obtained from different experimental realizations for a particular case of $\tau_{P1-P2} = 0.075$. However, for the very strongly interacting case shown later for e.g. $\tau_{P1-P2} = 0.025$ s, turbulence generation diminishes the repeatability to a large extent.

Figure 10 shows an interesting case of $\tau_{P1-P2} = 0.05$ s, and $t_{p,exp} = 0.03$ s. Here the time delay between the two vortices is smaller and a counterclockwise vortex is forced into an already existing clockwise circulation field. In the first few images of Fig. 10, apparently there is a Kelvin Helmholtz type of instability manifested by formation of multiple vortices with growing sizes. This phenomenon could be understood from the piston velocity time history for this case shown in Fig. 11. From, Fig. 12 it is clear that the velocity difference between the two fluid streams (air side and acetone seeded side) is growing which results in the formation of a Kelvin Helmholtz type instability with increasing amplitude. This increasing velocity difference causes a small timescale velocity perturbation which is superposed on the existing nominal velocity deficit across the mixing layer. This perturbation also leads
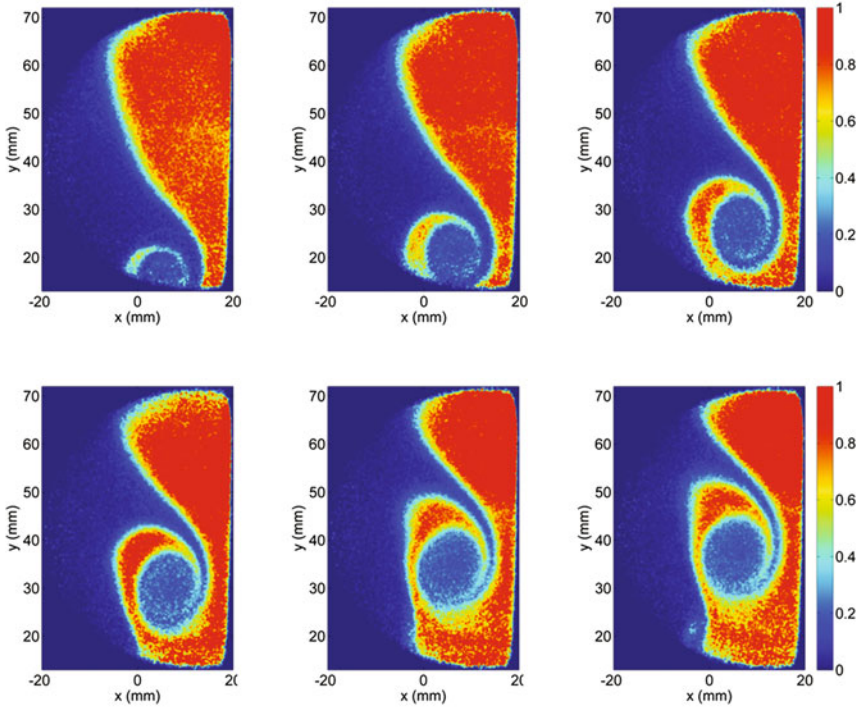
Fig. 7 PLIF profiles for air side pulsed vortex

to formation of small timescale eddy due to KH type instability. Finally when steady flow on the air side is reached, all the small vortices rotate as a part of a larger counterclockwise circulating field as shown in later images of Fig. 10. Figure 12 shows the simultaneous generation of two vortices $\tau_{P1-P2} = 0.025$ s, or $t_{p,exp} = 0.00$ s, which results in disorganized turbulent structures without any net circulation as might be expected from Biot Savart's law. Figure 13 shows the case where the air side pulse precedes the acetone side pulse with $\tau_{P1-P2} = 0.00$ s, and $t_{p,exp} = -0.025$ s. The experimental results provide a good insight into the general mixing and flow structures of the interacting vortices. It is imperative to use the computational model for a few selected cases to show quantitatively the main features of mixing in this type of vortical flow field.

4   Computational Results

The computational data are reported primarily for the following cases, (a) vortex pair with A1/A2 (pulse strength ratios of the two vortices)$= 1$ and 0.66 with a phase lag of $\tau = 1.4$ and (b) vortex couple with A1/A2 (pulse strength ratios of the two
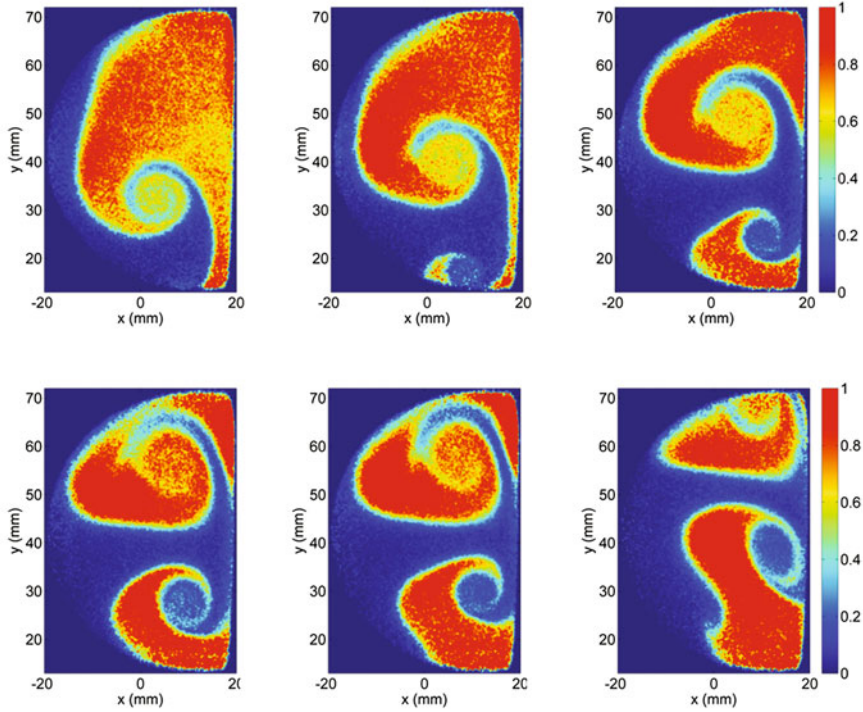
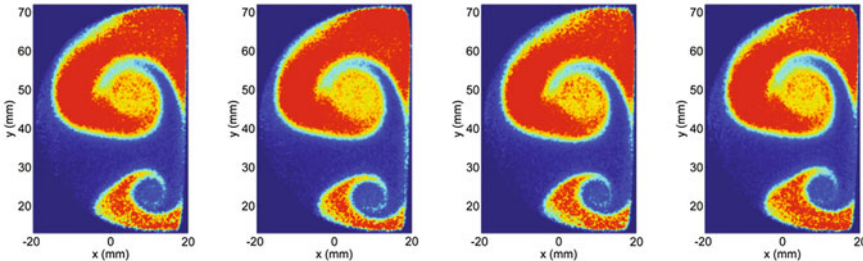**Fig. 8** $\Delta\tau_{P1-P2} = 0.075$ s

Fig. 9 Repeatability study of a particular mode of interaction for $\Delta\tau_{P1-P2} = 0.075$ s

vortices) $= 1$ and 0.66 with a phase lag of $\tau = 1.75$. The numerical conditions were chosen similar to the experimental conditions as possible in terms to phase delay. This represents a small subset of the experimental conditions. As described before the computational data shows reasonably good visual agreement with the experimental PLIF contours (Fig. 2). This gave us confidence to propose a mixing enhancement analysis based on probability density functions using the computational data to gain insight into the characteristics of species mixing in interacting vortices.
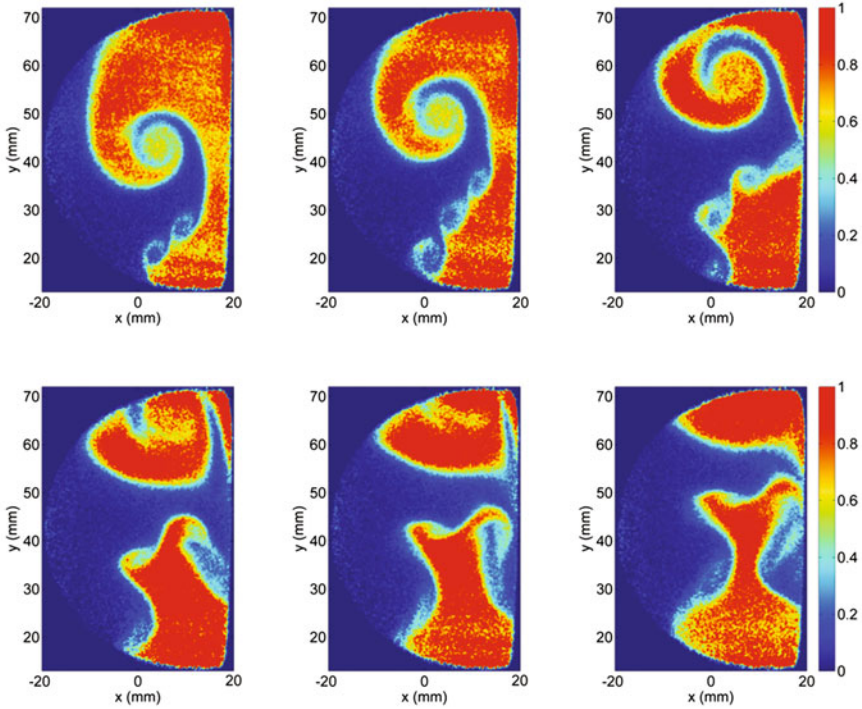
Fig. 10 $\Delta\tau_{P1-P2} = 0.050$ s

Figure 14a shows the temporal evolution of the species mass fraction profiles for vortices generated from opposite sides at a phase lag of $\tau_p = 1.4$. It can be seen that for the till $t^* = 8.4$ following the generation of the first pulse, the vortices show minimum interaction and predominantly show a single vortex. This is because even though the first vortex is strong at this point the second vortex is very weak due to the phase lag of $\tau_p = 1.4$. However after $t^* = 9$, both the vortices start showing strong interactions as exhibited in Fig. 14b. The first vortex is deformed by the rotation induced by the second vortex particularly in the vortical arms away from the vortex core. Significant thinning of the diffusion layer is also observed due to stretching induced by the counter rotating vortices. It is also observed that the walls obstruct the growth of the vortices leading to further thinning of the diffusion layer connecting the two vortices. Figure 14b shows the visual evidence of the growth of the vortices at different time instants. It is noticed that till $t^* = 9$, the vortex concentration profile matches closely the single vortex profile reported by Basu et al. [16]. However at later time instants, the second vortex closely interacts with the first and merges with one another. From $t^* = 16$ onwards, the cores of the two vortices become indistinguishable and represents a predominantly diffused core without any intricate windings of the vortical arms.
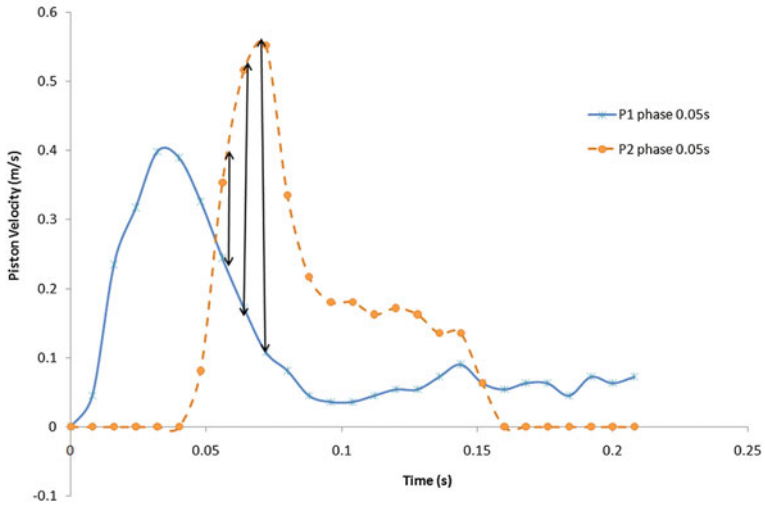
Fig. 11 Relative motions of P1 and P2 showing the increasing velocity difference between two pistons $\Delta\tau_{P1-P2} = 0.050$ s
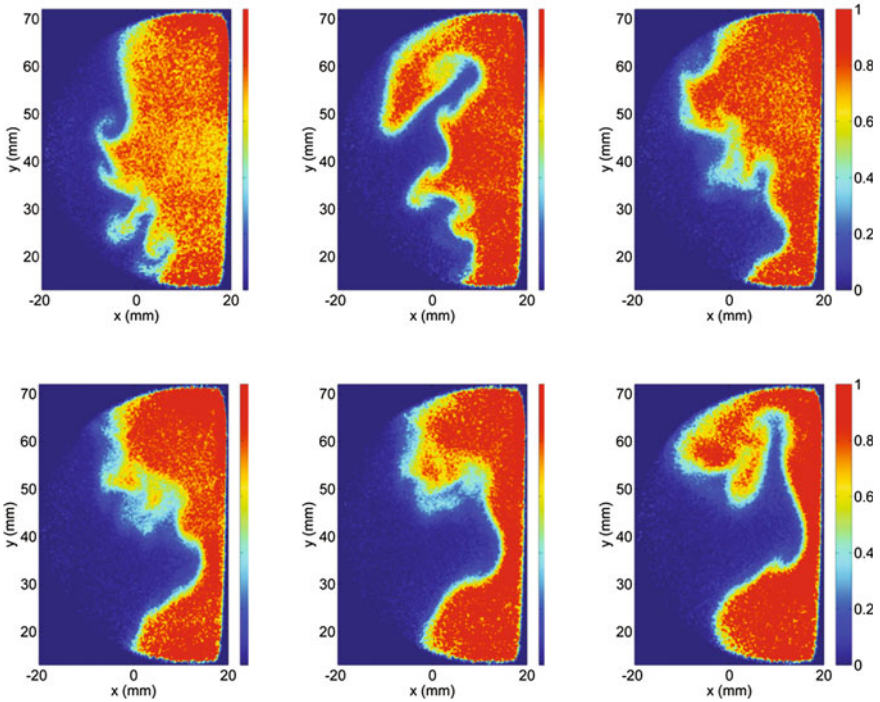

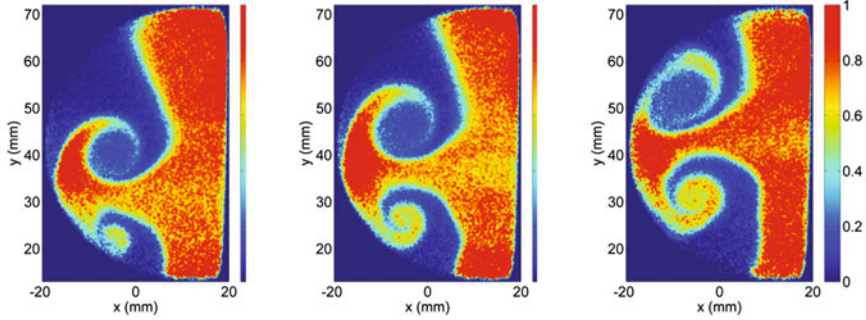**Fig. 12** $\Delta\tau_{P1-P2} = 0.025$ s

Fig. 13 $\Delta \tau_{P1-P2} = 0.000$ s

5   Mixing Enhancement Analysis

5.1   Probability Density Function Representation

The scalar mixing in the field of a vortex can be determined by evaluating the spatial probability density function (pdf) of the scalar concentration P(c) from spatial concentration distributions [17]. The pdfs were calculated over a spatial region (both lateral and streamwise extent) that is substantially larger than the total vortex span of the two interacting vortices [17]. These obtained pdfs are renormalized such that $\int_{c=0}^{c=1} P(c) = 1$ where c = 0 and c = 1 corresponding to the scalar concentrations in unseeded and seeded streams respectively. In Fig. 15 mean and variance of 'c' are compared for two different cases. These two parameters are defined as

$$\left. \begin{aligned} \bar{c} &= \frac{\int_{c=0}^{c=1} P(c) \cdot c \cdot dc}{\int_{c=0}^{c=1} P(c) \cdot dc} \\ c_{\mathrm{var}} &= \frac{\int_{c=0}^{c=1} P(c) \cdot (c - \bar{c})^2 \cdot dc}{\int_{c=0}^{c=1} P(c) \cdot dc} \end{aligned} \right\} \tag{5}$$

Further details of the methodology for calculating these two parameters have been discussed by Cetegen [8, 17] for isolated vortices. For both conditions $\bar{c}$ shows a self-similar trend. It maintains a constant value before the first pulse induces a vortical mixing which enhances $\bar{c}$. However, after the second pulse, the trend for $\bar{c}$ becomes different for vortex couples and pairs. For vortex pair (Fig. 14a), second pulse induces mixing in same direction which further increases the value of $\bar{c}$. On the other hand the vortex couple (Fig. 14b) induces a second vortex rotating in the opposite direction of the first vortex. This generates a secondary peak of high probability at lower concentration resulting in reduction of $\bar{c}$. c_{var} is a parameter which measures the non-uniformity of the seed concentration within the flow field. c_{var} plots shown in Fig. 15
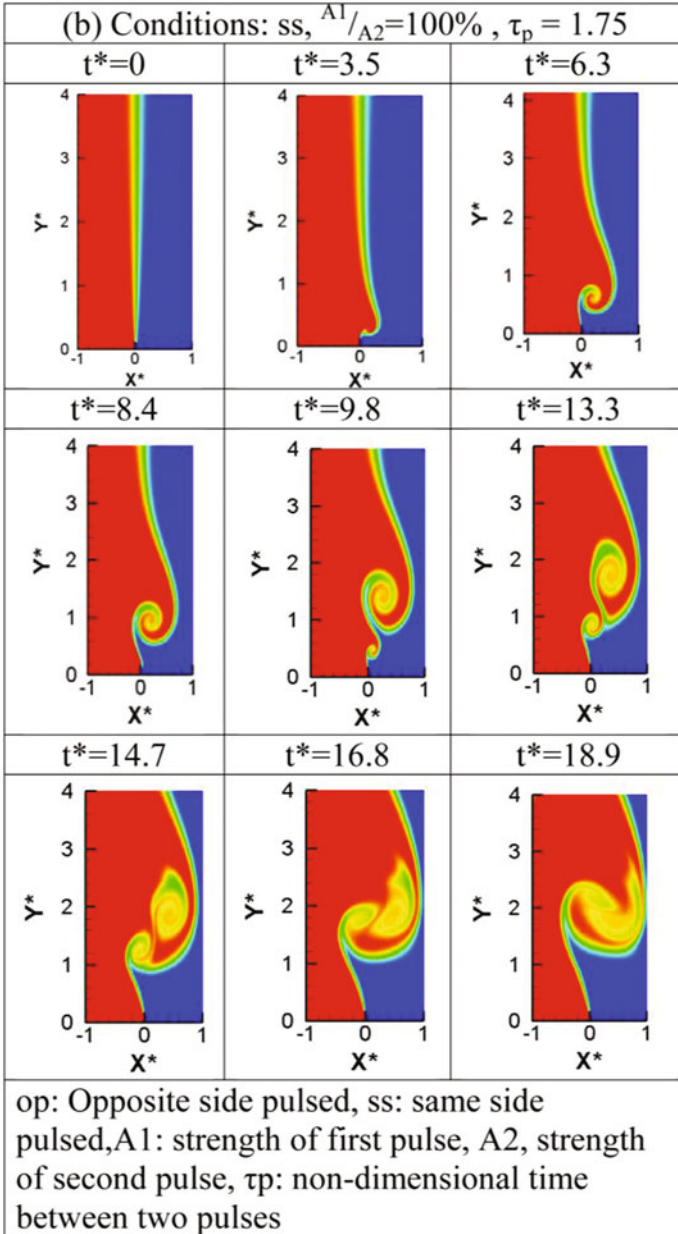
Fig. 14 Computational results: **a** A chronological visual representation of the interaction of two vortices (vortex couple) formed when seeded (acetone) and unseeded (air) sides were subsequently pulsed, **b** A chronological visual representation of the interaction of two vortices formed (vortex pair) when acetone (seeded side) was pulsed twice as the flow of air remained constant
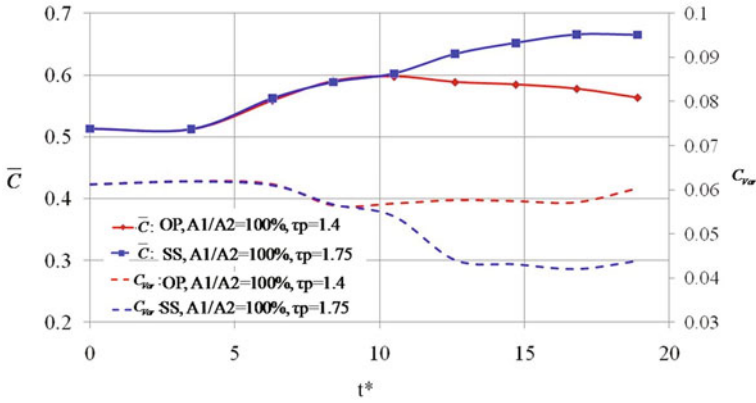
Fig. 15 Mean and variance of the scalar mass fraction c for different pulse strengths and time lags in the interacting vortices

suggest that c_{var} maintains almost a constant value for vortex couple, indicating that the mixing is very localized near the vortex cores. However, for vortex pair, a sharp decrease in the value of c_{var} is observed as the second vortex is generated. Although analysis with probability density function identifies global mixing patterns, it fails to correlate the effect of vorticity and corresponding mixing dynamics. This requires a different approach with conditional probability density function.

5.2 Conditional Probability Density Function

Statistical measures need to be introduced to quantify mixing in both molecular as well as advective sense for the interacting vortices while preserving their individual identities. This could be achieved, i.e. a high degree of mixing of a passive scalar in a vortical flow could be considered, if the following criteria are satisfied.

- The spatial gradients of the passive scalar have disappeared within the vortex i.e. a high degree of mixing can be considered to have occurred if species concentration gradients are low, indicating substantial diffusion has already taken place, a signature of molecular mixing. This can be observed in the scalar pdf when a single sharp peak is obtained at the intermediate levels of scalar concentration, suggesting homogeneity of the species concentration field. This is the conventional choice of reporting mixing behavior.
- Topologically, the species concentration and vorticity distribution functional forms are nearly similar for Schmidt numbers greater than unity. In other words, species concentration iso-lines which are spirals approach the shape of the circular vorticity iso-lines, indicating that sufficient advective transport of species have taken place. Motivated by the geometric similarity of the vorticity and species concentration

contour shapes a joint pdf of vorticity and species can be introduced to be a suitable marker of vortical mixing. This joint pdf can be suitably normalized by the pdf of vorticity to remove any ambiguity originating from considering the joint pdf which is dependent on many case specific parameters like area of interrogation, high vorticity regions not of interest in the current study such as boundary layers etc.

Thus for proper mixing both of the above mentioned criteria are satisfied if the probability density function $f(Y_i|\omega) \to 1$ in non-extremum species concentrations. For homogenous species and vorticity condition (say at very later stages of exponential decay of a Oseen vortex when $\omega \to 0$, and species field is nearly homogenous) the conditional probability function (cpdf) structures degenerates to a point in the typical contour plots as in Figs. 16 and 17 and attains a maximum attainable value of 1 indicating maximum degree of mixing. So, the cpdf is essentially a measure of mixing.

This is presented extensively in Figs. 16a, b and 18a, b for the different modes of interaction already mentioned to elucidate the evolution and nature of mixing in such interactions. Figure 16 presents as a matrix of individual images, where the first column shows species concentration iso-lines (black lines) superimposed with vorticity contours (jet color scale) in a rectangular region of interest selected within the computational domain at a particular instant of time. The time instants are reported on the left of the first columns for each row. The second column shows the corresponding cpdf of species concentration of acetone conditioned on vorticity at that time instant. Figure 16a shows the case of oppositely pulsed vortices of equal strength. At $t^* = 6.3$, the first row shows an unmixed state as evident from the low-magnitudes and non-coherent distribution of the cpdf. The subsequent time instants in Fig. 16a at $t^* = 10.5$, 14.7 and 18.9, progressively higher degree of mixing for the first vortex is observed in form of high levels of probability density in the negative vorticity regions of the cpdf. But in the last two images a second vortex with positive vorticity has entered the interrogation window. Even though visually its structure is similar to the first one at initial times, its vorticity is lower and is characterized by very weak mixing as observed from the time instants at $t^* = 14.7$ and 18.9. This is due the fact that the first vortex leaves a weakly rotational flow field, in which the second vortex is convected while rotating in opposite direction, i.e. vortex couple configuration. This substantially lowers its circulation strength and dissipates mixing even though the residual vorticity is weak and almost indiscernible in the contour images or the cpdf plots. This makes these mixing phenomena highly non-trivial and shows that it is strongly affected by prior history of vortex interaction. This mixing behavior is also unique as the cpdf has nearly same probability density over the entire range of species concentrations within the vortex: a feature which is not observed for the first vortex even at its initial stages. To substantiate this finding and to establish that this is due to effect of the first vortex and not a numerical artifact, a vortex with the exactly same parameters and pulsed at the same time instant and inlet velocity time histories but in the absence of a first vortex was simulated and its characteristics were compared with those of the second vortex. This is shown in Fig. 17 where we
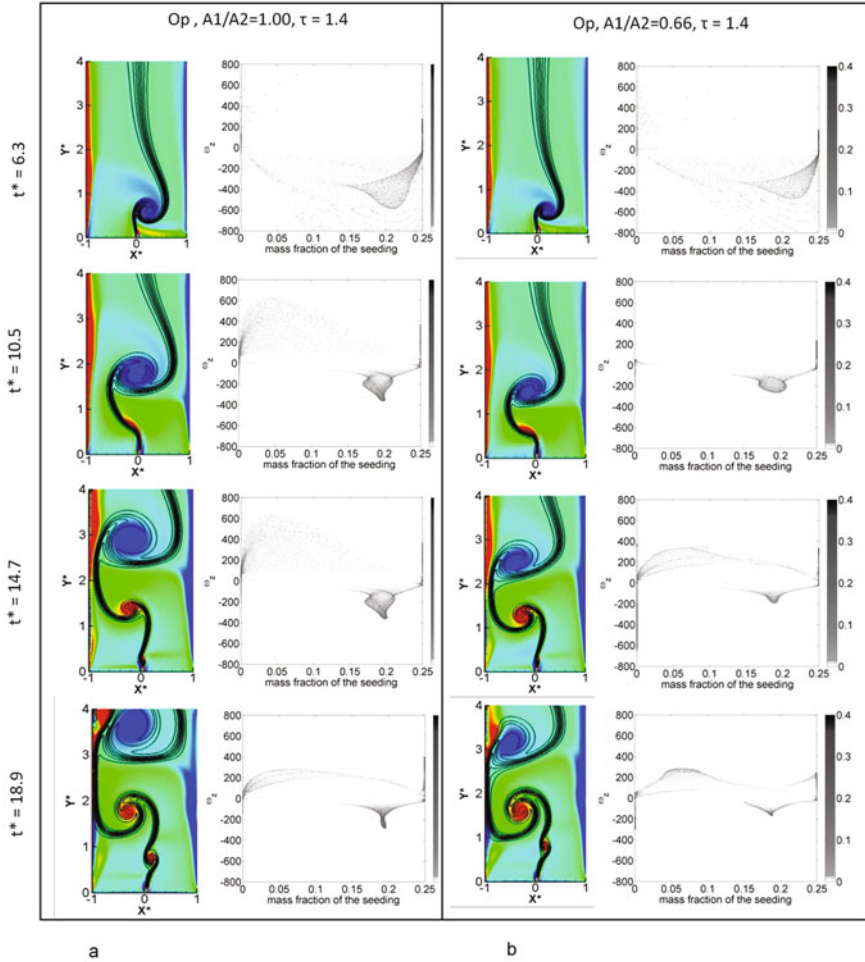
Fig. 16 Vortex couple: **a** Species concentration (mass fraction) isolines (black lines) superimposed with vorticity contours (jet color scale) in a rectangular region of interest selected within the computational domain at different time instants, **b** cpdf of concentration of seeding conditioned on vorticity at different time instants

observe a much higher degree of mixing for the individual vortex when it is not preceded by an oppositely rotating vortex. Figure 16b shows the contours and cpdfs of species concentration and vorticity for the oppositely pulsed but different pulse strength vortices. As observed from later stages of interaction at $t^* = 14.7$ and 18.9 mixing is slightly enhanced for the second vortex in comparison to the one for equal strength case (Fig. 16a $t^* = 14.7$ and 18.9) since the pulse strength for the preceding oppositely rotating vortex is reduced. If the counter-rotation was simultaneous it could be expected that vorticity would be damped by Biot Savart's law. However
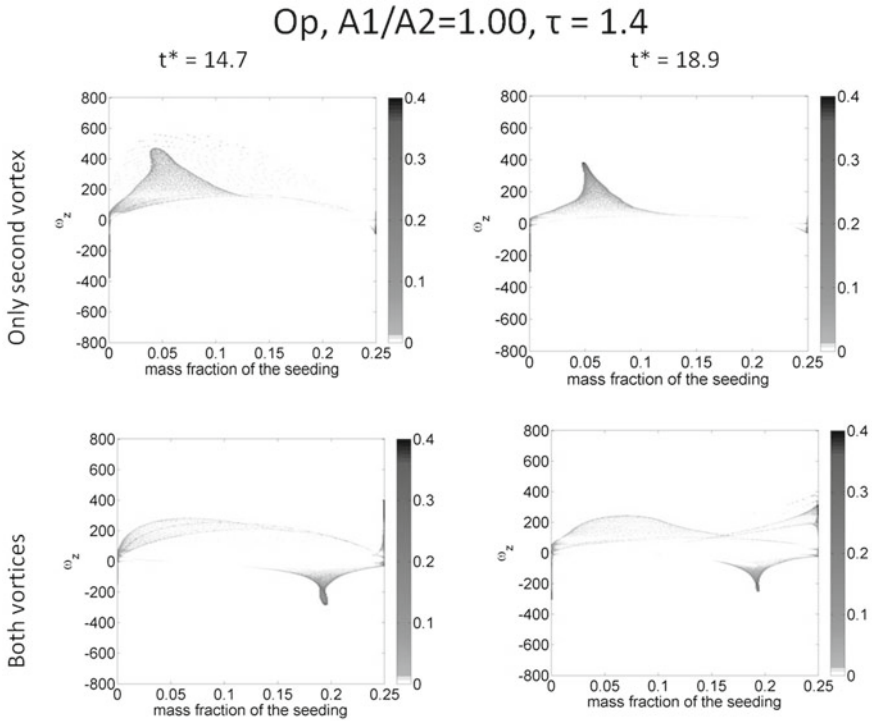
Op, A1/A2=1.00, τ = 1.4

Fig. 17 Comparison of the degree of mixing for single isolated vortex and interacting vortices

all the cases reported have a time lag such that the first vortex has convected and second vortex evolves in its decaying influence. Thus it can be concluded that even the exponentially decaying field of a "convecting" vortex is sufficiently strong to dissipate mixing in a subsequent vortex if it is rotating in an opposite direction, i.e. vortex couple configuration.

Enhancement of mixing occurs when a second vortex spins in the same direction as that of its predecessor, i.e. vortex pair configuration. This is shown in Fig. 18a and Fig. 18b with equal and unequal strengths respectively. Figure 18a at $t^* = 10.5$, 14.7 and 18.9 show that two cpdf structures evolve corresponding to two vortices produced, with the structure on the right corresponding to the first vortex and the one on the left corresponding to the second. Counterintuitive to the general understanding of the development and decay of a vortex, the second vortex shows higher degree of mixing though the first one had a longer development time and intuitively would have better mixing characteristics. However, once again the second vortex evolves in an already strained flow and scalar field as left behind by the roll up of the first vortex. Due to velocity induction the two vortices rotate about each other resulting in additional species advection. Moreover, due the close proximity of the two vortices, the first vortex essentially compresses the second vortex, resulting in higher straining
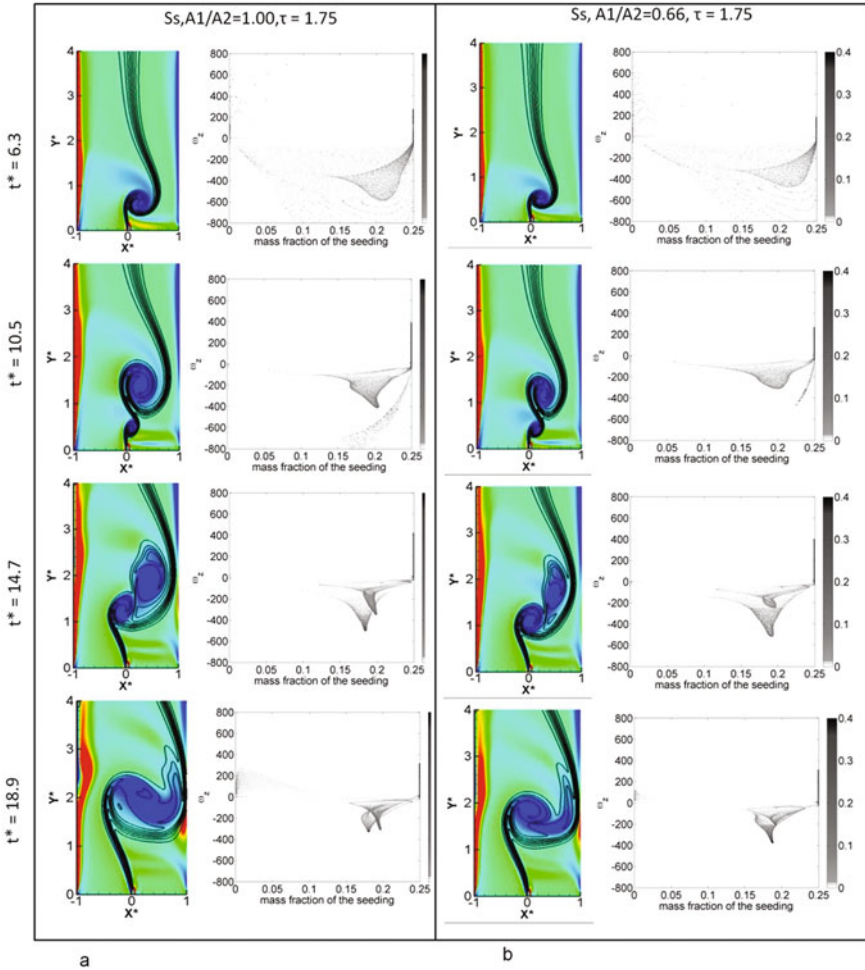
Fig. 18 Vortex pair: **a** Species concentration (mass fraction) isolines (black lines) superimposed with vorticity contours (jet color scale) in a rectangular region of interest selected within the computational domain at different time instants, **b** cpdf of concentration of seeding conditioned on vorticity at different time instants

of the second. This produces better mixing of the species in the second and hence higher probability densities in the cpdf. That the second vortex is better mixed than its isolated counterpart is evident by com-paring the two interaction time instants at $t^* = 14.7$ and 6.3. At around the same point of their evolution time, the strained second vortex at $t^* = 14.7$ is smaller in size with a more homogenous species field than the isolated one at $t^* = 6.3$. This characteristic was not evident without the mixing parameter which quantifies the degree of mixing for each of the structures. At a later time step as shown at $t^* = 18.9$ the cpdf structures approach each other closely

with similar mixing characteristics. Still, the second vortex shows a better mixed state as evident from the concentrated high value of the mixing parameter which suggests forced mixing within the second vortex by the first one. For the different pulse strength case shown in Fig. 18b, it is observed that the first vortex is distorted by the velocity induction effect of the second vortex hence the overall mixing is determined by that of the second as observed from the cpdfs at $t^* = 14.7$ and 18.9.

5.3 Strain Rate Analysis

Strain analysis in another approach used by different authors in the context of vortical mixing. In a vortical field molecular diffusion takes place in the interface of two streams of flow. This mixing is primarily caused by stretching and transportation of the interface of two fluids. The phenomena of stretching can be quantified in terms of strain rate, which is defined as, $\varepsilon = \frac{1}{l} \frac{\Delta l}{\Delta t}$, where l is the length, Δl change in length in Δt time and ε is the strain rate.

Figures 5, 6, 7, 8, 9, 10, 11, 12 and 14 show that seeded and un-seeded sides do not have a clear line interface due to molecular diffusion. It can be observed in the figures that concentration of acetone varies from 0 (air-side) to 0.25 (acetone-seeded side) at the interface of two streams. Therefore strain analysis has been performed on an iso-concentration line of 0.125, which is the average of maximum and minimum acetone concentrations within the flow field.

To calculate instantaneous strains, a numerical technique has been employed using MATLAB. Data files containing instantaneous concentration distribution within the flow field has been extracted from Fluent results. Subsequently, a numerical code has been used to find out the successive grid points having acetone concentration of 0.125. Linear distances between these grid points eventually results in the total length of iso-concentration line. A typical iso-contour line for an arbitrary time instance (t^j) has been shown in Fig. 19. The line has been constructed by joining all the grid points containing acetone concentration of 0.125. Following this, the code calculated the distances between successive nodes. For example, in Fig. 19, on the iso concentration line, two nodes have been shown as node k and node k + 1. In the inset, the nodes are zoomed into show the process of length calculation. The horizontal and vertical projection of the distance between two nodes, Δx_k and Δy_k has been found out by subtracting coordinates of two nodes.

$$\left.\begin{array}{l} \Delta x_k = x_{k+1} - x_k \\ \Delta y_k = y_{k+1} - y_k \end{array}\right\} \tag{6}$$

where x_k and y_k are co-ordinates of 'k'th node. The linear distance (Δl_k) between two nodes has been found out employing Pythagoras rule.

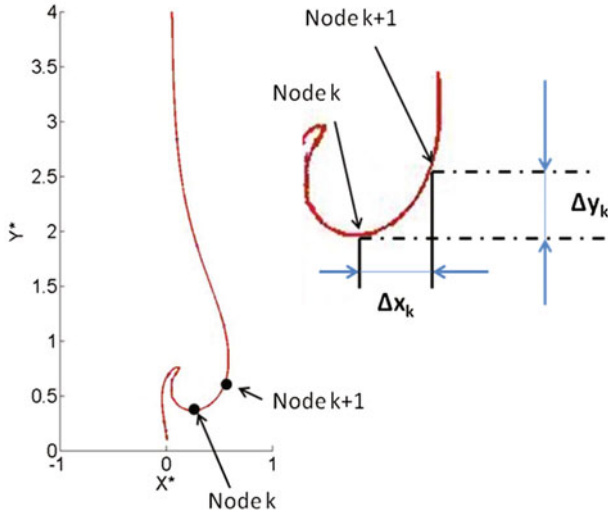$$\Delta l_k = \sqrt{(\Delta x_k)^2 + (\Delta y_k)^2} \tag{7}$$

Fig. 19 Process of calculating the iso-concentration lines

This process has been repeated for all nodes present on the iso concentration line and finally the total length of the line has been calculated by summing the values.

$$\left.\begin{aligned}
len_{xx} &= \sum_k |\Delta x_k| \\
len_{yy} &= \sum_k |\Delta y_k| \\
len &= \sum_k |\Delta l_k|
\end{aligned}\right\} \qquad (8)$$

where len_{xx} = horizontal (x-direction) projection of iso-concentration line, len_{yy} = vertical (y-direction) projection of iso-concentration line, len = length of iso-concentration line.

This method has been repeated for all time instances to calculate a progressive elongation of iso-concentration line. Figure 19 shows these iso-concentration lines at different time instances for condition of opposite side pulsed with same strength with time lag between pulses of $\tau_p = 1.4$.

After determination of instantaneous lengths, the strain has been calculated. It was necessary to calculate directional strain as well as total strain. They are calculated by the following formulae:

$$\left.\begin{array}{l} \varepsilon_{xx}^{j+1} = \dfrac{1}{len_{xx}^j} \dfrac{(len_{xx}^{j+1} - len_{xx}^j)}{(t^{j+1} - t^j)} \\[12pt] \varepsilon_{yy}^{j+1} = \dfrac{1}{len_{yy}^j} \dfrac{(len_{yy}^{j+1} - len_{yy}^j)}{(t^{j+1} - t^j)} \\[12pt] \varepsilon^{j+1} = \dfrac{1}{len^j} \dfrac{(len^{j+1} - len^j)}{(t^{j+1} - t^j)} \end{array}\right\} \quad (9)$$

where

len^j length of iso-concentration line at 'j'th time instant
len_{xx}^j horizontal (x-direction) projection of iso-concentration line at jth time instant
len_{xx}^j vertical (y-direction) projection of iso-concetration line at jth time instant
t^j absolute time at jth time instant
ε^j instantaneous total strain rate at jth time instant
ε_{xx}^j instantaneous horizontal (x-direction) strain rate at jth time instant
ε_{yy}^j instantaneous vertical (y-direction) strain rate at jth time instant.

5.3.1   Opposite Sides Pulsed, Same Pulse Strength, $\tau_p = 1.4$

Figure 20a depicts evolution of iso-concentration line for this condition. This figure clearly shows stretching of iso-concentration line in both horizontal (x) and vertical (y) direction. However, it can be observed that the stretching in horizontal direction is severe compared to other direction. Figure 20b shows temporal growth of iso-concentration line (*len*) and its two projections (*len_{xx}*, and *len_{yy}*). All the lines are observed to stretch with time. However, it can be noted that between $t^* = 5$ and 10 there is a rapid growth, which is artifact of initiation and development of the first vortex. Similarly, there is another phase of rapid growth at the later stage which corresponds to the second vortex. The two vortices are separated by a considerable amount of time, resulting in two distinct phase of higher growth rate. This has also been reflected in Fig. 19c, where the strain rates are compared. Both total strain (ε) and vertical strain (ε_{yy}) have two wide spread humps showing the effect of two vortices. Initially (at time $=0$) the iso-concentration line was vertical resulting in zero horizontal projection (*len_{xx}*). This has been reflected in Fig. 19c with very high initial horizontal strain rate (ε_{xx}). However, with time this strain rate decays. This is because flow structure gets trapped between two side walls limiting the potential to expand in horizontal direction.

5.3.2   Opposite Sides Pulsed, Weak First Pulse, $\tau_p = 1.4$

Evolution of iso-concentration line in Fig. 21a shows less vertical stretching compared to the case with same pulse strength. Figure 21b shows pattern of iso-concentration line and its projection at different time instances. It is evident that length of iso-concentration line (*len*) and vertical projection (*len_{yy}*) shows a smaller

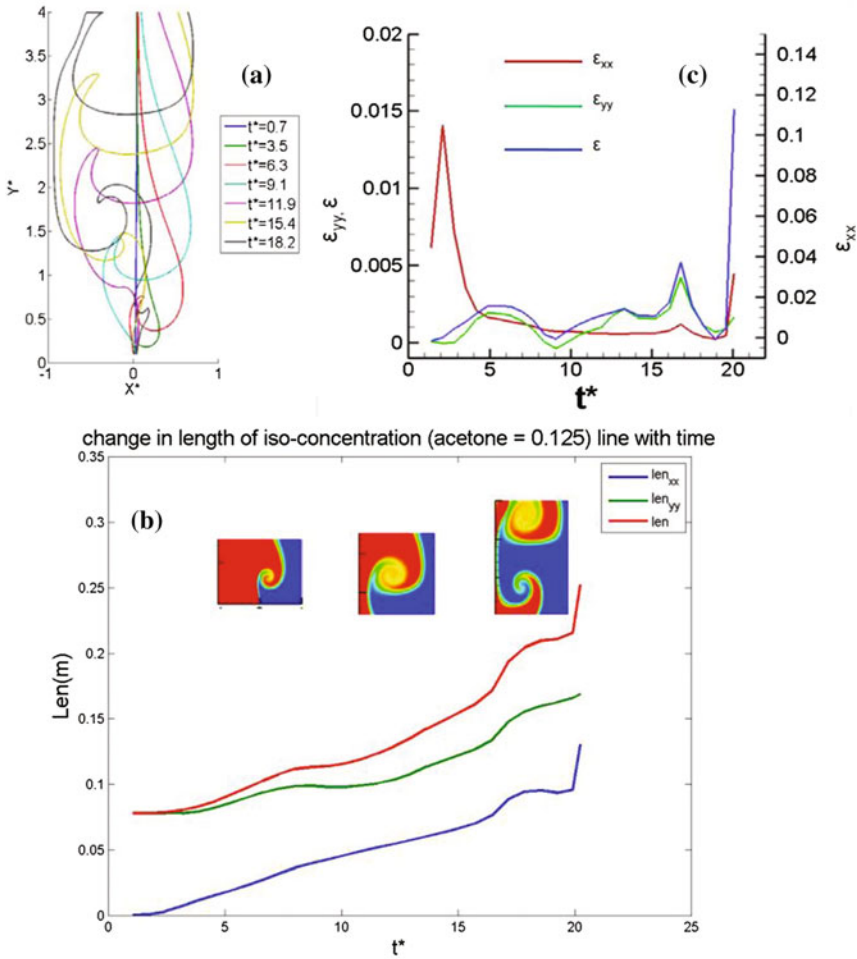**Fig. 20 a** Instantaneous iso-concentration (c = 0.125) line at different time instances, **b** change in iso-concentration length over time period with instantaneous vortex structure, **c** change in strain rates for Op, A1/A2 = 100%, $\tau_p = 1.4$

increase in growth during generation of first vortex, while later on they exhibit a faster growth during second vortex. This is because of the fact that first vortex is weaker compared to the second one. This phenomenon has been observed in strain rate plots as shown in Fig. 21c. Both ε and ε_{yy} showed two separate zones of higher strain rates. Each of them corresponds to two separate vortices. However, it can be noted that the increase in strain rate due to stretching of iso-concentration line is weaker in case of first vortex compared to the second one. Other component of strain rate, ε_{xx} shows a similar trend like previous cases. This strain rate gets limited due to the wall effect.
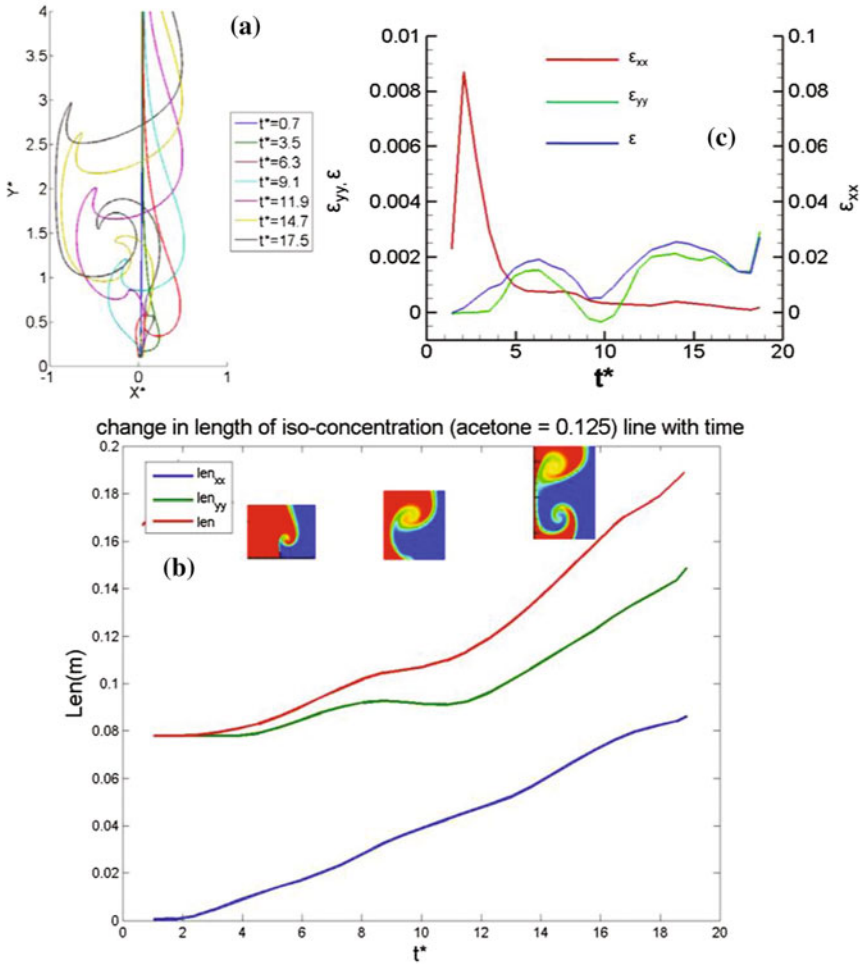
Fig. 21 **a** Instantaneous iso-concentration (c = 0.125) line at different time instances, **b** change in iso-concentration length over time period with instantaneous vortex structure, **c** change in strain rates for Op, A1/A2 = 66%, τp = 1.4

6 Summary

In this chapter we have investigated an interesting mixing phenomenon that arises from the interaction of two convecting line vortices generated at successive time instants. Same and opposite direction of rotation generating vortex pairs and couples augments and dissipates species mixing respectively as suggested by global scalar statistics like mean and variance. Local mixing due to vortical flow is investigated by introduction of a statistical parameter defined as cpdf of the scalar for a given vorticity.

This quantitatively shows how mixing is dissipated or augmented for individual vortices and at different vorticity magnitudes, even by the decaying and apparently indiscernible presence of a favorable or unfavorable direction of rotation of the preceding vortex. Since mixing is primarily caused by stretching and transportation of the interface of two fluids, detailed strain rate analysis of the iso-concentration lines shows phases of rapid growth corresponding to the initiation and development of the two vortices.

References

1. S.B. Pope, *Turbulent Flows* (Cambridge University Press, Cambridge, 2000)
2. F.E. Marble, Growth of a diffusion flame the field of a vortex, in *Recent Advances in Aerospace Sciences*, ed. by C. Casci, C. Bruno (Plenum, New York, 1985), pp. 395–413
3. A.R. Karagozian, F.E. Marble, Study of mixing and reaction in the field of a vortex. Combust. Sci. Technol. **45**, 65 (1986)
4. C.J. Rutland, J. Ferziger, Simulations of flame-vortex interactions. Combust. Flame **84**, 343 (1991)
5. J.C. Lee, C.E. Frouzakis, K. Boulouchos, Numerical study of opposed-jet H2/air diffusion flame—vortex interactions. Combust. Sci. Technol. **158**, 365 (2000)
6. A. Laverdant, S. Candel, A numerical analysis of a diffusion flame vortex interaction. Combust. Sci. Technol. **60**, 79 (1989)
7. A. Laverdant, S. Candel, Computation of diffusion and premixed flames rolled-up in vortex structures. J. Propul. Power **5**, 139 (1989)
8. B.M. Cetegen, W.A. Sirignano, Study of mixing and reaction in the field of a vortex. Combust. Sci. Technol. **72**, 157 (1990)
9. N. Peters, F.A. Williams, Premixed combustion in a vortex, in *Symposium (International) on Combustion*, vol. 22, pp. 495 (1988)
10. P.H. Renard, D. Thevenin, J.C. Rolon, S. Candel, Dynamics of flame/vortex interactions. Prog. Energy Combust. Sci. **26**, 225 (2000)
11. E. Villermaux, J. Duplat, Mixing as an aggregation process. Phys. Rev. Lett. **91**, 18 (2003)
12. P. Meunier, E. Villermaux, How vortices mix. J. Fluid Mech. **476**, 213–222 (2003)
13. K. Bajer, A.P. Bossom, A. Gilbert, Accelerated diffusion in the center of a vortex. J. Fluid Mech. **437**, 395–411 (2001)
14. M. Long, M.A. Sprague, A.A. Grimes, B.D. Rich, M. Khine, Appl. Phys. Letts **94**, 133501 (2009)
15. K. Sritharan, C.J. Strobl, M.F. Schneider, A. Wixforth, Z. Guttenberg, Appl. Phys. Lett. **88**, 054102 (2006)
16. S. Basu, T.J. Barber, B.M. Cetegen, Computational study of scalar mixing in the field of a gaseous laminar line vortex. Phys. Fluids **19**, 053601 (2007)
17. B.M. Cetegen, Scalar mixing in the field of a gaseous laminar line vortex. Exp. Fluids **40**, 967 (2006)